

Wave-packet continuum discretization approach to He^{2+} -He collisions

Sh. U. Alladustov ^{1,*}, C. T. Plowman ¹, I. B. Abdurakhmanov ², I. Bray ¹ and A. S. Kadyrov ^{1,†}

¹*Department of Physics and Astronomy and Curtin Institute for Computation, Curtin University,
GPO Box U1987, Perth, Western Australia 6845, Australia*

²*Pawsey Supercomputing Centre, 1 Bryce Avenue, Kensington, Western Australia 6151, Australia*



(Received 24 September 2022; revised 2 December 2022; accepted 5 December 2022; published 21 December 2022)

The two-center wave-packet convergent close-coupling method is generalized to multiply charged ion collisions with helium and applied to the He^{2+} -He scattering problem. The approach is applicable in a wide range of collision energies including low and intermediate energies, where coupling between various reaction channels and electron exchange between the fragments in the rearrangement channel are important. The target structure is treated using the configuration-interaction method within the frozen-core approximation, where one of the electrons of the target is assumed to stay in the ground state throughout the collision. This accounts for the indistinguishability and the correlations between the electrons of the target. We also use a simpler alternative method that is based on an effective one-electron target description that neglects the electron-electron correlations. In both methods, the continuum of the target atom and the hydrogenlike atom formed after electron capture by the projectile is discretized using the wave-packet approach. We present cross sections for total and state-selective electron capture, excitation, and single ionization of the target. The results are provided for the incident energies from 10 keV/u to 5 MeV/u, where one-electron processes are expected to dominate. Particular attention is focused on the intermediate-energy region where substantial deviations between various theoretical results are found. However, overall, the present results are in good agreement with experimental data and other calculations, where available. We demonstrate that both effective single-electron and two-electron methods can provide a realistic picture of all single-electron scattering processes taking place in He^{2+} -He collisions in terms of the total cross sections. This creates a reliable platform for modeling differential scattering and ionization in this four-body system.

DOI: [10.1103/PhysRevA.106.062819](https://doi.org/10.1103/PhysRevA.106.062819)

I. INTRODUCTION

In atomic physics, collisions of fully stripped ions with helium are of particular interest. Studying the underlying processes in such four-body scattering systems has essential applications in a wide range of fundamental sciences such as astrophysics and plasma physics. These collisions are also relevant to hadron therapy of cancer [1], where bare ions are used to deliver a required dose of radiation to destroy tumor cells. Recent reviews of ion-atom collisions and their applications are provided in Refs. [2,3]. The importance of studying collisions involving multiply charged ions with large nuclear charges is that they can deliver higher doses of radiation than protons due to their larger masses. For these and many other reasons, scattering of various singly and multiply charged ions on helium has been extensively investigated both theoretically [4–15] and experimentally [16–27].

Theoretically, describing ion collisions with the helium atom is very challenging due to the two-electron nature of the target. The corresponding Schrödinger equation for the target atom cannot be solved analytically and the accuracy

of solutions highly depends on the approximations and numerical approaches applied. Therefore, some authors ignore the electron-electron correlation effects by employing the independent-electron model (IEM) in their approaches [14,28–30]. In this method, the active electron moves independently in the potential generated by the interaction with the residual target (He^+). The IEM approach is more efficient. Its use is justified at the collision energies where the electron-electron correlation is negligible.

Scattering problems involving the helium atom provide a sensitive test for theoretical methods. Depending on the projectile energy, a wide range of theories were employed to investigate collisions of bare ions with helium with varying success. One of the successful models to describe ion-atom collisions is the corrected first Born (CB1) approximation first introduced within the three-body formalism by Belkić *et al.* [31]. The method overcomes the issue of residual long-range Coulomb interactions by introducing the correct Coulomb boundary conditions in the entrance and exit channels. The CB1 method was applied to the four-body problem of fully stripped ion collisions with heliumlike atoms. Applications of the four-body boundary-corrected first Born (CB1-4B) approximation were reported in Refs. [5,9,12,13] for the helium target. In particular, for the He^{2+} projectile, the results agreed very well with measurements at intermediate and high energies.

*sh.alladustov@gmail.com

†a.kadyrov@curtin.edu.au

The boundary-corrected four-body version of the continuum-distorted-wave theory was developed by Belkić *et al.* [32] and later was successfully applied to calculate single-electron-capture cross sections in various ion-atom collision systems including He^{2+} -He scattering in Ref. [33]. Another distorted-wave theory is the continuum-distorted-wave eikonal-initial-state (CDW-EIS) approach [34,35]. Generalization of the CDW-EIS approach, which uses a more accurate description of the states, was developed by Abufager *et al.* [30]. Calculated cross sections for electron capture in He^{2+} -He collisions showed good agreement with the experimental data. Terekhin *et al.* [35] used the three-body CDW-EIS method to study electron capture and ionization in multiply charged ion collisions with helium. The results agreed well with the experimental data; especially at high impact energies, agreement was very good. Samaddar *et al.* [36] applied the four-body model of target continuum-distorted-wave approximation to study scattering of protons and α particles on helium in the energy range from 30 to 1000 keV/u. Very recently, Delibašić *et al.* [37] tabulated total and state-selective cross sections for single-electron capture from the helium atom in its ground state by a number of multiply charged ions using the three-body boundary-corrected continuum intermediate state (BCIS-3B) method at intermediate and high projectile energies.

At sufficiently high energies the probability of electron capture is small in comparison with the probabilities of excitation and ionization. Therefore, excitation and ionization in He^{2+} -He collisions can be described using a single-center atomic-orbital coupled-channel (CC) method. Barna *et al.* [38] and Pindzola *et al.* [39] showed that the single-center CC approach can adequately describe the ionization process above 600 keV/u. Their results showed good agreement with the experimental data available in this energy region.

The classical trajectory Monte Carlo (CTMC) approach, based on numerically solving the corresponding Hamilton equations, is another widely used method in ion-atom collisions. The CTMC method cannot be directly applied to study the scattering problems involving helium and other multielectron atoms due to the instability of the target description. This problem, in the case of the helium target, was overcome by several means: (i) Stabilizing potentials were employed. Zajfman and Maor [7] in their work used the Heisenberg uncertainty principle to stabilize the helium atom to study collisions of bare ions with helium. (ii) The target was treated as a one-electron system by neglecting the electron-electron correlation. This approach was applied to study various post-collisional processes in proton and antiproton scattering on helium by Schultz and Olson [15]. (iii) Dynamical screening was introduced for the initially bound electrons (DCTMC). The DCTMC method was developed by Montemayor and Schiwietz [40] and Meng *et al.* [41] for the helium target. It was applied to calculate the total and state-selective electron-capture cross sections in He^{2+} -He collisions by Alessi *et al.* [17]. Their results agreed well with experimental measurements.

Along with their CC calculations, Barna *et al.* [38] presented two versions of the CTMC methods. They used an equivalent electron (EE) and a nonequivalent electron (NEE) approximation to study single and double ionization of helium

by heavy-particle impact. In the first approach, the problem was treated as a four-body system, where the electron-electron interaction was neglected and two electrons were treated as nonequivalent. The helium wave functions were built as products of two different single-particle wave functions. In the second method, a system of three particles (the projectile, the active electron, and the remaining He^+ ion) was considered. The two-electron wave functions were constructed as products of two identical single-particle wave functions. The NEE-CTMC method was shown to agree better with the experiment than the EE-CTMC one; however, both methods were not as successful as the CC method for the purpose of investigating the ionization process.

A method based on the time-dependent density-functional theory (TDDFT) was developed by Baxter and Kirchner [42] to study collisions involving helium atoms. They used a multiconfiguration Hartree-Fock (MCHF) ground-state helium wave function. Within the framework of TDDFT, the results of two models, one based on the Wilken-Bauer (WB) correlation integral model and the other on an independent-electron model (IEM), were compared and the TDDFT WB method was shown to have an advantage over the TDDFT IEM one. In particular, the TDDFT WB method significantly improved agreement between theory and experiment for the total electron-capture cross section in the problematic region below 100 keV/u.

Close-coupling approaches, which use atomic or molecular orbitals as basis functions in the expansion of the electronic time-dependent scattering wave function, are also commonly applied to study ion-atom collisions. The atomic-orbital close-coupling (AOCC) approach was employed in Refs. [43,44] to study collisions of He^{2+} ions with the ground state or metastable helium atom. In [43], He^{2+} -He collisions were studied at low and intermediate projectile energies, where electron-electron interactions were taken into account. Particular attention was paid to obtaining partial cross sections for single transfer, transfer-excitation, and excitation of the target, which are sensitive to the target description. The one-electron model of the method was applied to collisions with metastable helium. A fully correlated two-active-electron semiclassical atomic-orbital close-coupling method was recently applied to collisions of multiply charged ions with helium [45]. The advantage of this method is that it uses a large basis, takes the interaction of electrons into account, and includes a set of pseudostates. One of the successful approaches to studying very-low- to low-energy ion-atom collisions is the quantum-mechanical orbital close-coupling (QMOCC) method [46]. The QMOCC method applied to He^{2+} -He collisions [47,48] showed good agreement with the experimental data.

The wave-packet convergent close-coupling (WP-CCC) approach was developed by Abdurakhmanov *et al.* [49]. It has been applied to various three-body scattering problems including multiply charged projectiles [50–52]. The approach is based on discretizing the continuum by subdividing it into a certain number of bins. Within each bin, square-integrable states are constructed by integrating the continuum eigenfunction. For four-body scattering problems involving the helium target, the WP-CCC method was introduced by Abdurakhmanov *et al.* [53,6] to study scattering of antiprotons

and energetic protons on helium within the frozen-core framework. Later we extended the method to include electron capture in proton-helium collisions [54]. One of the important features of the two-center method is that it accounts for the electron exchange between the fragments in the rearrangement channels, particularly important at low energies. In the four-body WP-CCC approach, the wave packets for the target are constructed using the helium continuum functions obtained by numerically solving the corresponding Schrödinger equation. For single-electron capture, single ionization, and excitation of the target, the results showed good agreement with available experimental data and other calculations. Recently, the method was applied to proton-helium differential scattering problems [55,56]. At intermediate collision energies, the calculations of angular differential cross sections for elastic scattering, target excitation, electron capture, and various singly differential cross sections for ionization agreed with experimental measurements very well. The WP-CCC approach has recently been extended to the proton-H₂ system as well [57,58].

In this paper we extend the two-center four-body WP-CCC approach, originally developed for p -He collisions [54], to multiply charged ion collisions with helium and apply it to the He²⁺-He scattering problem. This is an example of a four-body scattering problem with the residual long-range Coulomb interaction in the rearrangement channel. We present total electron-capture, excitation, and single-ionization cross sections for He²⁺-He collisions. There are many experimental measurements and other theoretical calculations of the integrated cross sections for the considered processes and we make comparisons wherever available. Furthermore, we present state-selective electron-capture cross sections into the $1s$, $2s$, $2p$, $3s$, $3p$, and $3d$ states of the hydrogen-like He⁺ ion formed after electron capture. State-selective capture cross sections are compared with the calculations of Mančev *et al.* [59], but there are not enough experimental works for comparison. For the He²⁺ projectile, the scarcity of experimental data can be explained by the fact that after the electron is captured by He²⁺, the formed and the residual ions (both are He⁺ ions) become indistinguishable, which makes the state-selective measurements more challenging. In this work we pay particular attention to the intermediate-energy region due to its relevance to the ITER and JET fusion projects.

Unless specified otherwise, atomic units (a.u.) are used throughout this paper.

II. THEORY

A. The WP-CCC approach with a correlated two-electron description of the target

Here we describe the two-center WP-CCC approach to $P^{(Z)}$ -He collisions, where $P^{(Z)}$ is a fully stripped projectile ion of charge Z (for He²⁺, $Z = 2$). We follow Refs. [60,61], where a similar extension was performed for one-electron targets. The total scattering wave function Ψ is the solution of the Schrödinger equation

$$(H - E)\Psi = 0, \quad (1)$$

where H is the full four-body Hamiltonian. The total energy E can be written in any one of the three forms

$$\begin{aligned} E &= E_0 + \frac{k_\alpha^2}{2\mu_T} + \epsilon_\alpha \\ &= E_0 + \frac{k_{1\beta}^2}{2\mu_P} + \epsilon_{1\beta}^{(Z)} \\ &= E_0 + \frac{k_{2\beta}^2}{2\mu_P} + \epsilon_{2\beta}^{(Z)}, \end{aligned} \quad (2)$$

with E_0 the binding energy of the frozen target electron. The indices α and β denote the full set of quantum numbers representing states in the $P^{(Z)}$ -He and $P^{(Z-1)}$ -He⁺ channels, respectively. Channel 1β is the same as channel 2β but with the electron of the residual target and that of the $P^{(Z-1)}$ ion exchanged. Furthermore, k_α is the momentum of the projectile relative to the helium atom in the α channel, μ_T is the reduced mass of this system, ϵ_α is the energy of the pseudostate α , $k_{1\beta}$ (and $k_{2\beta}$) is the momentum of the formed $P^{(Z-1)}$ ion relative to the residual helium ion in the 1β (2β) channel, μ_P is the reduced mass, and $\epsilon_{1\beta}^{(Z)}$ ($\epsilon_{2\beta}^{(Z)}$) is the energy of the hydrogenlike ion $P^{(Z-1)}$ in the 1β (2β) channel. We note that $\epsilon_{1\beta}^{(Z)} = \epsilon_{2\beta}^{(Z)}$.

The full Hamiltonian H can be represented in three equivalent forms

$$H = K_\sigma + H_{T_1} + H_{T_2} + V_P + V_{12} \quad (3)$$

$$= K_{\rho_1} + H_{P_1} + H_{T_2} + V_1 + V_{12} \quad (4)$$

$$= K_{\rho_2} + H_{P_2} + H_{T_1} + V_2 + V_{12}, \quad (5)$$

where kinetic energy operators are defined as

$$K_\sigma = -\frac{\nabla_\sigma^2}{2\mu_T}, \quad K_{\rho_i} = -\frac{\nabla_{\rho_i}^2}{2\mu_P}, \quad i = 1, 2 \quad (6)$$

and Coulomb interaction potentials as

$$V_P = \frac{2Z}{R} - \frac{Z}{x_1} - \frac{Z}{x_2}, \quad (7)$$

$$V_1 = \frac{2Z}{R} - \frac{2}{r_2} - \frac{Z}{x_1}, \quad (8)$$

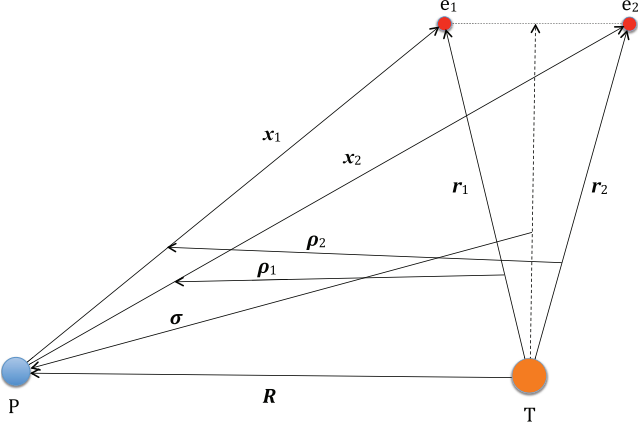
$$V_2 = \frac{2Z}{R} - \frac{2}{r_1} - \frac{Z}{x_2}, \quad (9)$$

$$V_{12} = \frac{1}{|\mathbf{r}_1 - \mathbf{r}_2|}. \quad (10)$$

The vectors \mathbf{R} , \mathbf{r}_1 , and \mathbf{r}_2 define the positions of the incident projectile and the two electrons relative to the origin, respectively, \mathbf{x}_1 and \mathbf{x}_2 are the position vectors of the helium electrons relative to the projectile, $\boldsymbol{\sigma}$ is the position vector of the projectile relative to center of mass of the helium atom, and $\boldsymbol{\rho}_1$ ($\boldsymbol{\rho}_2$) is position vector of the system of the projectile and the first (second) electron relative to the helium ion (see Fig. 1). The Hamiltonians of the $P^{(Z-1)}$ ion and the He⁺ ion formed by each of the target electrons are written as

$$H_{P_i} = -\frac{\nabla_{x_i}^2}{2} - \frac{Z}{x_i}, \quad i = 1, 2 \quad (11)$$

$$H_{T_i} = -\frac{\nabla_{r_i}^2}{2} - \frac{2}{r_i}, \quad i = 1, 2, \quad (12)$$

FIG. 1. Jacobi coordinates for the He^{2+} -He system.

respectively. With these definitions the Hamiltonian of the helium atom is written as

$$H_T = H_{T_1} + H_{T_2} + V_{12}. \quad (13)$$

We employ an impact-parameter method in modeling the collisional system, which assumes that the target nucleus is fixed at the origin and the incident projectile is moving along the straight-line trajectory $\mathbf{R} \equiv \mathbf{R}(t) = \mathbf{b} + \mathbf{v}t$, where \mathbf{b} is the impact parameter and \mathbf{v} is the initial velocity of the projectile. We set the z axis along \mathbf{v} . The vector \mathbf{b} is set perpendicular to the direction of the moving projectile, i.e., $\mathbf{b} \cdot \mathbf{v} = 0$.

The results of close-coupling approaches are dependent on the choice of the expansion of the total scattering wave functions. In our two-center WP-CCC approach, the scattering wave function is expanded in terms of N target-centered and M projectile-centered pseudostates as

$$\begin{aligned} \Psi = & \sum_{\alpha=1}^N F_{\alpha}(t, \mathbf{b}) \psi_{\alpha}^{\text{He}}(\mathbf{r}_1, \mathbf{r}_2) e^{i\mathbf{k}_{\alpha}\sigma} \\ & + \frac{1}{\sqrt{2}} \sum_{\beta=1}^M G_{\beta}(t, \mathbf{b}) [\psi_{\beta}^{(Z)}(\mathbf{x}_1) \psi_{1s}^{\text{He}^+}(\mathbf{r}_2) e^{i\mathbf{k}_{1\beta}\rho_1} \\ & + \psi_{\beta}^{(Z)}(\mathbf{x}_2) \psi_{1s}^{\text{He}^+}(\mathbf{r}_1) e^{i\mathbf{k}_{2\beta}\rho_2}], \end{aligned} \quad (14)$$

where $\psi_{\alpha}^{\text{He}}$ and $\psi_{\beta}^{(Z)}$ are the wave functions for the helium atom and $P^{(Z-1)}$, the hydrogenlike atom of nuclear charge Z formed after electron capture by the projectile, respectively. The helium wave functions $\psi_{\alpha}^{\text{He}}$ and energy levels are obtained by numerically solving the Schrödinger equation corresponding to the helium atom using the symmetric expansion $\psi_{\alpha}^{\text{He}}(\mathbf{r}_1, \mathbf{r}_2) = \psi_{\alpha}(\mathbf{r}_1) \psi_{1s}^{\text{He}^+}(\mathbf{r}_2) + \psi_{\alpha}(\mathbf{r}_2) \psi_{1s}^{\text{He}^+}(\mathbf{r}_1)$. The wave function $\psi_{1s}^{\text{He}^+}$ represents the ground state of He^+ . For their detailed definitions, refer to Refs. [54,62]. The expansion coefficients $F_{\alpha}(t, \mathbf{b})$ and $G_{\beta}(t, \mathbf{b})$ as $t \rightarrow +\infty$ represent the transition probability amplitudes into the various target and projectile states.

Next we insert the expansion in Eq. (14) into Eq. (1) and apply the semiclassical approximations. Then we successively multiply it by the pseudostates and integrate over all variables except for σ , ρ_1 , and ρ_2 to get a system of differential

equations for the time-dependent coefficients:

$$\begin{aligned} i\dot{F}_{\alpha'} + i \sum_{\beta=1}^M \dot{G}_{\beta} K_{\alpha'\beta}^T &= \sum_{\alpha=1}^N F_{\alpha} D_{\alpha'\alpha}^T + \sum_{\beta=1}^M G_{\beta} Q_{\alpha'\beta}^T, \\ i \sum_{\alpha=1}^N \dot{F}_{\alpha} K_{\beta'\alpha}^P + i \sum_{\beta=1}^M \dot{G}_{\beta} L_{\beta'\beta}^P &= \sum_{\alpha=1}^N F_{\alpha} Q_{\beta'\alpha}^P + \sum_{\beta=1}^M G_{\beta} D_{\beta'\beta}^P, \\ \alpha' &= 1, 2, \dots, N, \quad \beta' = 1, 2, \dots, M. \end{aligned} \quad (15)$$

Here the direct-scattering matrix elements are defined as

$$L_{\beta'\beta}^P = \frac{1}{2} \sum_{i,j=1,2} \langle \mathbf{k}_{i\beta'}, \psi_{\beta'}^{(Z)}, \psi_{1s}^{\text{He}^+} | \psi_{\beta}^{(Z)}, \psi_{1s}^{\text{He}^+}, \mathbf{k}_{j\beta} \rangle, \quad (16)$$

$$D_{\alpha'\alpha}^T = \langle \mathbf{k}_{\alpha'}, \psi_{\alpha'}^{\text{He}} | H_T - E_{\alpha}^{\text{He}} + V_P | \psi_{\alpha}^{\text{He}}, \mathbf{k}_{\alpha} \rangle, \quad (17)$$

$$\begin{aligned} D_{\beta'\beta}^P &= \frac{1}{2} \sum_{i,j=1,2} \langle \mathbf{k}_{i\beta'}, \psi_{\beta'}^{(Z)}, \psi_{1s}^{\text{He}^+} | H_{Pi} - \epsilon_{\beta}^{(Z)} | \psi_{\beta}^{(Z)}, \psi_{1s}^{\text{He}^+}, \mathbf{k}_{j\beta} \rangle \\ &+ \frac{1}{2} \sum_{i,j=1,2} \langle \mathbf{k}_{i\beta'}, \psi_{\beta'}^{(Z)}, \psi_{1s}^{\text{He}^+} | V_i | \psi_{\beta}^{(Z)}, \psi_{1s}^{\text{He}^+}, \mathbf{k}_{j\beta} \rangle \end{aligned} \quad (18)$$

and the rearrangement matrix elements are of the forms

$$K_{\beta'\alpha}^P = \frac{1}{\sqrt{2}} \sum_{i=1,2} \langle \mathbf{k}_{i\beta'}, \psi_{\beta'}^{(Z)}, \psi_{1s}^{\text{He}^+} | \psi_{\alpha}^{\text{He}}, \mathbf{k}_{\alpha} \rangle, \quad (19)$$

$$K_{\alpha'\beta}^T = \frac{1}{\sqrt{2}} \sum_{i=1,2} \langle \mathbf{k}_{\alpha'}, \psi_{\alpha'}^{\text{He}} | \psi_{\beta}^{(Z)}, \psi_{1s}^{\text{He}^+}, \mathbf{k}_{i\beta} \rangle, \quad (20)$$

$$Q_{\beta'\alpha}^P = \frac{1}{\sqrt{2}} \sum_{i=1,2} \langle \mathbf{k}_{i\beta'}, \psi_{\beta'}^{(Z)}, \psi_{1s}^{\text{He}^+} | H_T - E_{\alpha}^{\text{He}} + V_P | \psi_{\alpha}^{\text{He}}, \mathbf{k}_{\alpha} \rangle, \quad (21)$$

$$Q_{\alpha'\beta}^T = \frac{1}{\sqrt{2}} \sum_{i=1,2} \langle \mathbf{k}_{\alpha'}, \psi_{\alpha'}^{\text{He}} | H_{Pi} - \epsilon_{\beta}^{(Z)} + V_i | \psi_{\beta}^{(Z)}, \psi_{1s}^{\text{He}^+}, \mathbf{k}_{i\beta} \rangle, \quad (22)$$

where $E_{\alpha}^{\text{He}} = E_0 + \epsilon_{\alpha}$ is the energy of He in channel α and $\epsilon_{\beta}^{(Z)} \equiv \epsilon_{1\beta}^{(Z)} = \epsilon_{2\beta}^{(Z)}$ is the energy of the hydrogenlike atom of nuclear charge Z .

We assume that the active electron of helium is initially in the ground state; therefore, the above system of equations is solved subject to the initial boundary condition

$$\begin{aligned} F_{\alpha}(-\infty, \mathbf{b}) &= \delta_{\alpha,1s}, \quad \alpha = 1, \dots, N \\ G_{\beta}(-\infty, \mathbf{b}) &= 0, \quad \beta = 1, \dots, M. \end{aligned} \quad (23)$$

The transition probability amplitudes $F_{\alpha}(+\infty, \mathbf{b})$ and $G_{\beta}(+\infty, \mathbf{b})$ are obtained by solving the system of differential equations (15) as $t \rightarrow +\infty$. This is performed using the standard Runge-Kutta technique over a finite z grid from $-z_{\text{max}}$ to $+z_{\text{max}}$, where z_{max} was set to 200 a.u. This requires accurately calculated matrix elements at each time step. These amplitudes are used to find the probability of the active electron, after the collision, to be in the direct-scattering channel α or in the rearrangement channel β ,

$$P_{\alpha}(b) = |F_{\alpha}(+\infty, \mathbf{b}) - \delta_{\alpha,1s}|^2, \quad (24)$$

$$P_{\beta}(b) = |G_{\beta}(+\infty, \mathbf{b})|^2, \quad (25)$$

respectively. The obtained probabilities for the required range of impact parameters are used to calculate partial direct-scattering (DS) and electron-capture (EC) cross sections

$$\sigma_{\alpha}^{\text{DS}} = 2\pi \int_0^{b_{\text{max}}} db b P_{\alpha}(b), \quad (26)$$

$$\sigma_{\beta}^{\text{EC}} = 2\pi \int_0^{b_{\text{max}}} db b P_{\beta}(b), \quad (27)$$

where b_{max} , the upper limit for the impact-parameter range, is chosen to be sufficiently high, as detailed below. The total electron-capture cross section is the sum of the cross sections for transitions into the negative-energy eigenstates of the helium ion projectile:

$$\sigma^{\text{EC}} = \sum_{\beta, \epsilon_{\beta}^{(Z)} < 0} \sigma_{\beta}^{\text{EC}}. \quad (28)$$

The total single-ionization (SI) cross section is the sum of the partial cross sections for excitation into the positive-energy pseudostates of the target and electron transfer into the continuum of the projectile:

$$\sigma^{\text{SI}} = \sum_{\alpha, \epsilon_{\alpha} > 0} \sigma_{\alpha}^{\text{DS}} + \sum_{\beta, \epsilon_{\beta}^{(Z)} > 0} \sigma_{\beta}^{\text{EC}}. \quad (29)$$

B. The WP-CCC approach with effective one-electron treatment of the target

The correlated two-electron target description used in the preceding section is theoretically complex. It ultimately leads to scattering equations, the solving of which is computationally demanding. Recently, we have developed a simpler technique which models the target as an effective one-electron system. Details of the theory are given in Ref. [63] and its application to the helium target is described in Refs. [55,56].

Briefly, we first generate an accurate ground-state wave function for the target using a computational atomic-structure package that is based on the multiconfiguration Hartree-Fock approximation. Then we calculate the probability density for the target system before averaging over the electronic spin and the spatial coordinates of all but one electron, thus obtaining a single-electron density function which represents the probability of finding one electron at a certain distance from the nucleus. The single-electron wave function is then obtained by taking the square root of this function. Then the multielectron Schrödinger equation is reduced to an effective one-electron equation by inserting this wave function and we can inversely solve it to determine the effective potential that represents the collective field of the nucleus and all other electrons. Finally, using this numerical potential, we can generate excited states and a non-normalizable continuum state for the active electron. This is achieved using an iterative Numerov approach to solve the Schrödinger equation for the effective one-electron system. Positive-energy pseudostates representing the continuum are constructed using the wave-packet approach. This involves integration of the helium continuum-state wave function over a set of discretization bins [63].

Ultimately, we obtain a set of orthonormal pseudostates for the helium atom in an effective one-electron representation. While this makes computations significantly easier, the

method neglects the correlation effects between the electrons that become particularly important at lower impact energies. In addition, there is no electron exchange in the $\text{He}^+ \text{-He}^+$ channel as the residual target ion He^+ is effectively a single particle. For comparison, here we show results from both approaches.

Hereafter, we refer to the simplified effective one-electron method as E1E WP-CCC and the more accurate two-electron method that takes into account the correlation between the target electrons and exchange effects simply as WP-CCC.

III. RESULTS

In both approaches, the accuracy of the predictions depend on several factors such as the accuracy of the helium wave functions and corresponding energy levels, as well as the matrix elements. This was carefully taken care of in providing the final results. For example, calculated energy levels of the helium atom described the experimental data very well. Moreover, we studied the dependence of the cross sections on the number of discretization bins N_c , the maximum energy of the ejected electron ϵ_{max} , the maximum principal quantum number of negative-energy states n_{max} , and the maximum angular momentum quantum number l_{max} of all the included states. Systematic calculations were performed to test the convergence of the results by gradually increasing the number of both target-centered and projectile-centered states while maintaining the accuracy of the employed wave functions for the states. As mentioned in the preceding section, the resulting cross sections depend also on the choice of b_{max} , the upper limit for the impact parameter. In our calculations we set $b_{\text{max}} = 15$, which was sufficient to produce reliable integrated cross sections. Increasing this parameter further had no significant effect on the final results. To get accurate results and better convergence in terms of positive-energy pseudostates, the maximum energy of the included bin states, ϵ_{max} , needs to be large enough. Correspondingly, to obtain sufficiently dense bin states, the number of bins needs to be increased as ϵ_{max} gets larger. Taking these into consideration, ϵ_{max} ranged from 8 to 32 a.u. depending on the incident projectile energy.

In calculations, for simplicity we used an equal number of basis functions centered around the target and projectile. For given values of N_c , n_{max} , and l_{max} , the total number of states in each basis is found as

$$N = \sum_{l=0}^{l_{\text{max}}} (n_{\text{max}} + N_c - l)(2l + 1). \quad (30)$$

Setting $n_{\text{max}} = 5$ and $l_{\text{max}} = 3$ was shown to be sufficient to get stable results and increasing these values further did not show any significant changes. The convergence of the cross sections in terms of the number of bin states was achieved with $N_c = 20$ at lower and intermediate energies and with $N_c = 30$ at higher energies. The bases with these parameters consist of the 366 and 526 functions, respectively.

Below we present integrated cross sections for total and state-selective electron capture and excitation as well as single ionization in $\text{He}^{2+} \text{-He}$ collisions at incident energies from 10 keV/u to 5 MeV/u where one-electron processes are expected to dominate, with particular emphasis on the

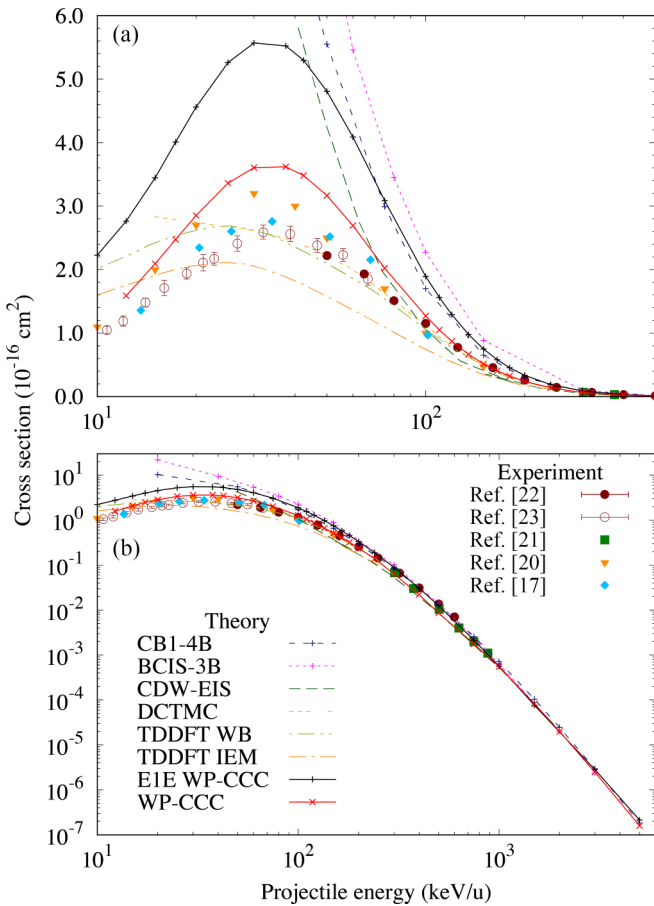


FIG. 2. Total cross section for electron capture in $\text{He}^{2+} + \text{He}(1s^2)$ collisions as a function of the incident projectile energy. The present two-electron and E1E WP-CCC results are represented by the red and black solid lines, respectively. The experimental data are due to Rudd *et al.* [20], Shah and Gilbody [22], Shah *et al.* [23], de Castro Faria *et al.* [21], and Alessi *et al.* [17]. The other theoretical results are from the BCIS-3B method by Delibašić *et al.* [37], the CB1-4B method by Mančev *et al.* [59], the CDW-EIS method by Abufager *et al.* [30], the DCTMC method by Alessi *et al.* [17], and the TDDFT WB and TDDFT IEM methods by Baxter and Kirchner [42] with MCHF. In (a) the low-energy region is highlighted using a linear scale. The error bars reported in Ref. [22] are too small to be visible.

intermediate-energy region. Here and hereafter, the incident energy is given in the laboratory frame where the target is at rest. The two-electron and E1E WP-CCC results are shown by the crosses and pluses, respectively. The calculated points are connected by solid lines to guide the eye.

A. Total and state-selective electron capture

In Fig. 2 the two-electron and E1E WP-CCC total cross sections for single-electron capture in $\text{He}^{2+} + \text{He}$ collisions are compared with the corresponding experimental data [17,20–23] and other theoretical results [30,37,42,43,59]. The experimental data are only available below 1 MeV/u. The cross section falls sharply at high energies; therefore, it is customary to depict it in a logarithmic scale. Figure 2(b), which covers a wide energy range using the logarithmic scale, shows that

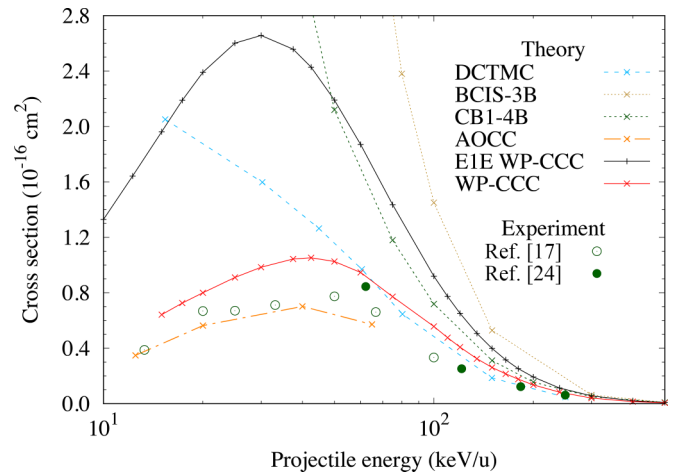


FIG. 3. State-selective electron-capture cross sections into the $1s$ state of He^+ in $\text{He}^{2+} + \text{He}(1s^2)$ collisions as a function of the incident projectile energy. The WP-CCC and E1E WP-CCC results are represented by the red and black solid lines, respectively. The experimental data are due to Alessi *et al.* [17] and Mergel *et al.* [24]. The DCTMC calculations by Alessi *et al.* [17], the BCIS-3B ones by Delibašić *et al.* [37], the CB1-4B results by Mančev *et al.* [59], and the AOCC results by Fritsch [43] are also shown.

there is very good agreement between all the theoretical calculations and the experimental measurements above 200 keV/u.

Thus, we can conclude that the high-energy electron-capture problem is fairly well understood as far as the integrated cross section is concerned. However, the situation is less clear in the intermediate-energy region highlighted in Fig. 2(a) using a linear scale. As one can see, there is significant deviation among the theoretical results. As expected, the high-energy perturbative methods [30,37,59] substantially overestimate the experimental data in this region. On the other hand, nonperturbative methods [42] predict dumping of the cross section as energy decreases. The present results produce the maximum of the cross section to be around 35 keV/u, in agreement with the measurements. However, both two-electron and E1E WP-CCC methods overestimate the experimental data near the maximum of the cross section. Not surprisingly, the two-electron WP-CCC method performs better as it accounts for the electron-electron correlation and electron-exchange effects. The deviation from the data by Rudd *et al.* [20] is about 15% at most. This can be considered reasonably good agreement given the fact that the deviation between the two sets of independent measurements by Rudd *et al.* [20] and Shah *et al.* [23] reaches 25%. The two sets of results by Baxter and Kirchner [42] based on the WB and IEM implementations of the TDDFT method are similar in shape, with the TDDFT WB method giving a systematically larger cross section than the TDDFT IEM one, in better agreement with experiment, at all energies. The DCTMC calculations are in very good agreement with the experiments [22,23] starting from 30 keV/u. Overall, we can see that the two-electron WP-CCC and TDDFT WB calculations are in better agreement with the experimental data in the entire energy range considered.

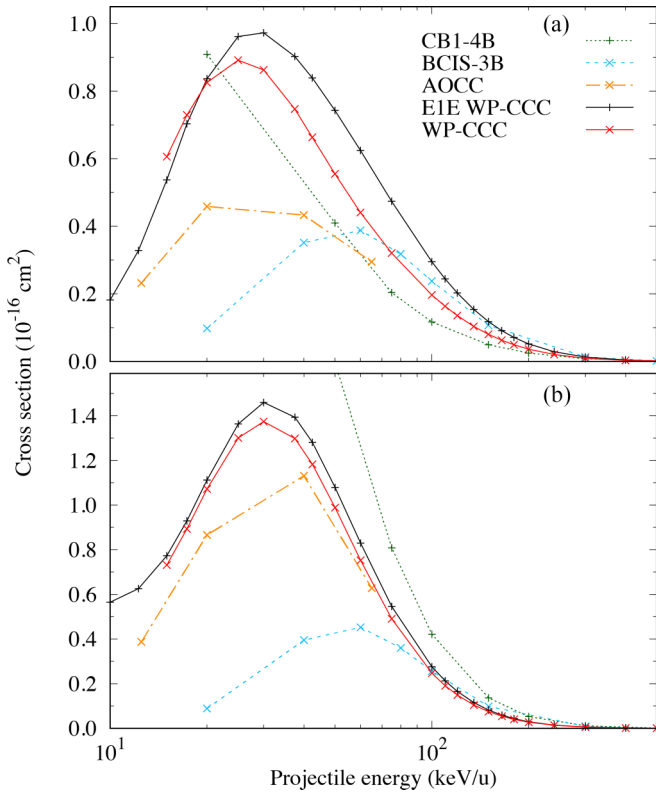


FIG. 4. State-selective electron-capture cross sections into the (a) $2s$ and (b) $2p$ states of He^+ in $\text{He}^{2+} + \text{He}(1s^2)$ collisions as a function of the incident projectile energy. The WP-CCC and E1E WP-CCC results are represented by the red and black solid lines, respectively. Other theoretical results are from the CB1-4B method by Mančev *et al.* [59], the BCIS-3B method by Delibašić *et al.* [37], and the AOCC method by Fritsch [43].

Further we concentrate on the intermediate-energy region and compare some of the state-selective electron-capture cross sections with other calculations and experimental data, where available. Figure 3 represents the cross sections for electron capture into the ground state of the He^+ ion. Our two-electron and E1E WP-CCC results are compared with the experimental data by Alessi *et al.* [17] and Mergel *et al.* [24] and the DCTMC [17], CB1-4B [59], BCIS-3B [37], and AOCC [43] calculations. The figure exposes a huge discrepancy between various theoretical methods for this important capture channel. The two-electron WP-CCC results are overall in fairly good agreement with the experimental data, while the E1E WP-CCC ones significantly overestimate the data near its maximum, highlighting the importance of accounting for the electron-electron correlation and electron-exchange effects. The AOCC method of Fritsch [43], which also takes the interaction of the electrons into account, is the only theory that agrees well with the experimental data of Alessi *et al.* [17]; however, the results are available only below 65 keV/u. We can also see that DCTMC calculations of Alessi *et al.* [17] overestimate the two-electron WP-CCC results at lower energies; however, they are in good agreement with our data above 60 keV/u.

In Figs. 4 and 5 the two-electron and E1E WP-CCC calculations for capture into excited states are compared with

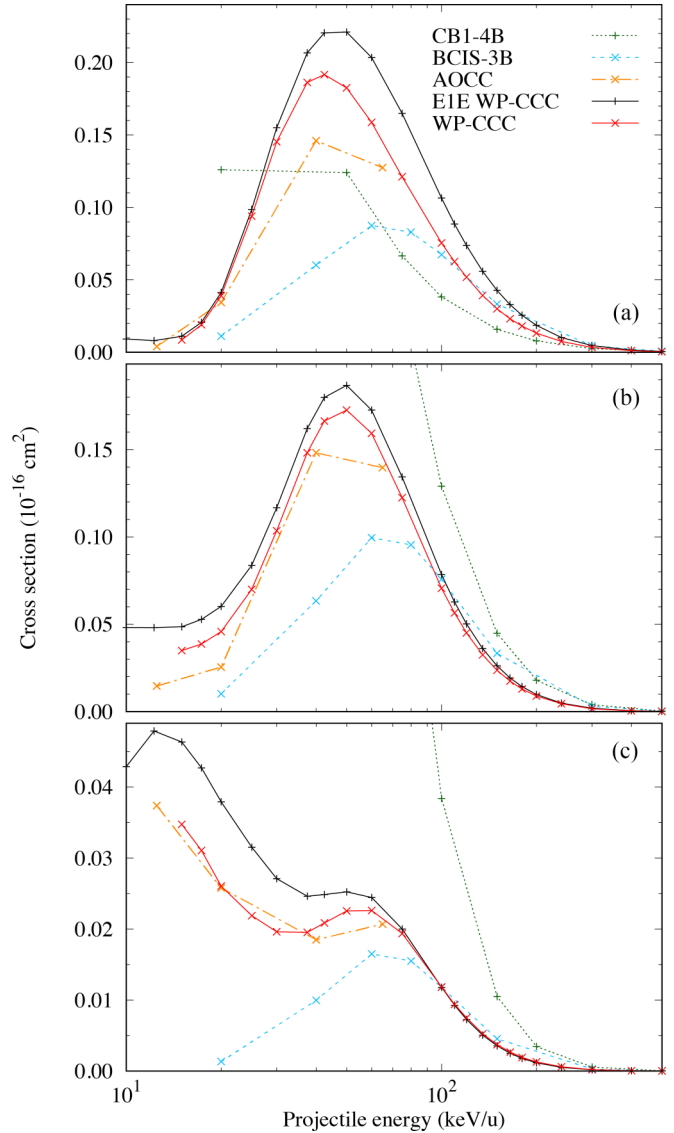


FIG. 5. Same as in Fig. 4 but for the (a) $3s$, (b) $3p$, and (c) $3d$ states.

the similar results based on the CB1-4B method by Mančev *et al.* [59] and the BCIS-3B one by Delibašić *et al.* [37]. The cross sections for the $2s$ and $2p$ states are shown in Fig. 4 and the results for the $3l$ states are presented in Fig. 5, summed over the magnetic quantum numbers where applicable. Again, Fig. 4 reveals substantial discrepancy between various theoretical methods for these dominant $n = 2$ capture channels. We emphasize, however, that all the methods are in excellent agreement with each other at high energies not only for the total cross section [see Fig. 2(b)] but also for practically all the state-selective cross sections (not shown). We can see substantial deviations for the $n = 3$ capture channels as well; however, the two-electron WP-CCC and the AOCC are in reasonably good agreement except for the capture into the $3s$ state, where the WP-CCC results are much higher. It can be seen that the E1E cross sections somewhat overestimate the two-electron WP-CCC ones at intermediate energy region, but the difference is not as high as it was for the ground

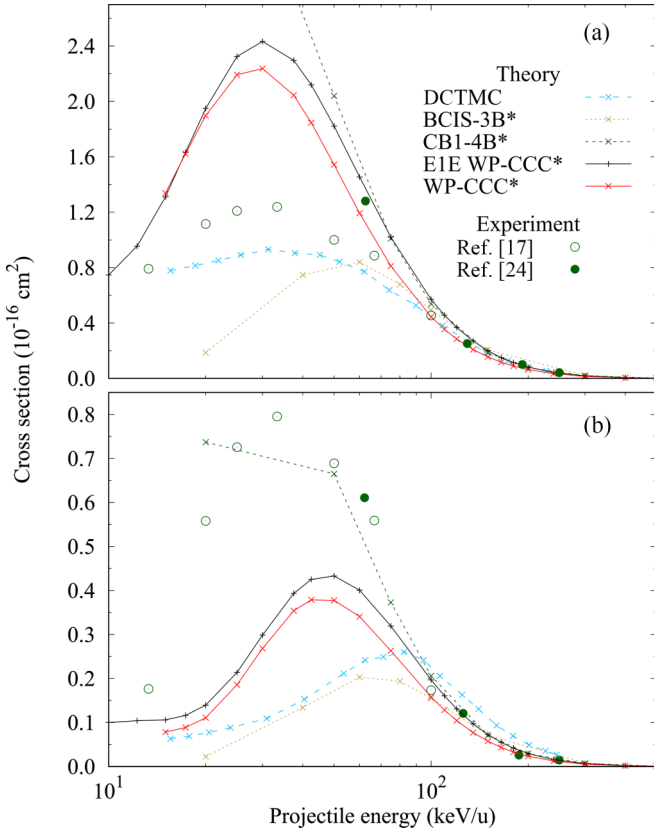


FIG. 6. State-selective electron-capture cross sections for the $\text{He}^{2+}\text{-He}(1s^2) \rightarrow \text{He}^+(n)\text{-He}^+(n')$ processes (see the text) for (a) $(2, 1) + (1, 2)$ and (b) $(3, 1) + (1, 3)$. The experimental data are due to Alessi *et al.* [17] and Mergel *et al.* [24]. The experiments do not distinguish which ion He^+ is in the excited state. The DCTMC calculations by Alessi *et al.* [17], the BCIS-3B ones by Delibašić *et al.* [37], and the CB1-4B results by Mančev *et al.* [59] are also shown. The asterisk after the method name indicates that the corresponding calculations include the contributions from the $\text{He}^{2+}\text{-He}(1s^2) \rightarrow \text{He}^+(n)\text{-He}^+(n' = 1)$ channels only.

state. The results from all the methods merge as the incident energy increases above 200 keV/u. Another observation is that both two-electron and E1E WP-CCC calculations for electron capture into the $3d$ state show oscillatory behavior at low energies, where there is no clear maximum.

Figure 6 shows the cross sections for electron capture into the $n = 2$ and 3 shells (summed over the orbital angular momentum and magnetic quantum numbers). We use the notation suggested by Mergel *et al.* [24] to denote the states of the ion formed by the projectile after electron capture and the residual target ion in the final channel. In this notation, (n, n') indicates the $\text{He}^{2+}\text{-He}(1s^2) \rightarrow \text{He}^+(n)\text{-He}^+(n')$ process. We contrast our results against the experimental data by Alessi *et al.* [17] and Mergel *et al.* [24] for the $(n, n') + (n', n)$ process, meaning that the experiments do not distinguish which He^+ ion is in the excited state. When the reaction products are symmetric, like in the $(1,2)$ and $(2,1)$ processes, their experimental separation becomes very challenging. Therefore, for $n = 2$ and 3, the experiments provide data for the sum of the cross sections for electron capture and residual target-ion excitation into the corresponding shell. We emphasize that

the DCTMC calculations [17] shown in the figure are for the $(n, n') + (n', n)$ process; however, our results and the CB1-4B [59] and BCIS-3B [37] ones correspond to the $(n, 1)$ case. As one can see from the figure, our E1E and two-electron WP-CCC results for the $(2,1)$ channel agree with the experimental data for $(2, 1) + (1, 2)$ starting from 60 keV/u. For the $(3,1)$ channel agreement with the experimental data for $(3, 1) + (1, 3)$ is seen starting from 100 keV/u. This allows us to conclude that above 60 and 100 keV/u the dominant contribution to the cross section of the $(2, 1) + (1, 2)$ and $(3, 1) + (1, 3)$ processes come from the $(2,1)$ and $(3,1)$ channels, respectively. A similar conclusion was drawn by Alessi *et al.* [17] with regard to the $(2, 1) + (1, 2)$ process where the $(2,1)$ channel was shown to be dominant. We also note that there is fair agreement between our two approaches throughout the entire energy range; especially at high energies, the agreement is very good. The DCTMC results for the $(2, 1) + (1, 2)$ process roughly follow the experimental data even at low energies; however, they completely fail to reproduce the data for the DCTMC $(3, 1) + (1, 3)$ process. Figure 6(b) appears to suggest that the CB1-4B [59] method better describes the $(3, 1) + (1, 3)$ data at 20 and 50 keV/u. However, the agreement is accidental since, first, the CB1-4B results are for the $(3,1)$ process only and, second, the method is known to significantly overestimate the state-selective electron-capture cross sections at these energies. Overall, there is clearly a need for better modeling the $(n, n') + (n', n)$ process. This should include developing a method that is capable of incorporating two-active-electron processes, like capture of one electron with simultaneous excitation of the residual target ion. Naturally, such a method should also include capture of one electron with simultaneous ionization of the residual ion.

The WP-CCC cross sections for electron capture into the $n = 1\text{--}5$ shells of the He^+ ion are tabulated in Table I. The total electron-capture cross section which is obtained by summing the cross sections into all these shells (and presented in Fig. 2) is also tabulated. Our results reveal that at lower energies the highest contribution is due to the $n = 2$ shell. However, starting from 80 keV/u, electron capture into the ground state becomes dominant. It should also be noted that at projectile energies above 0.5 MeV/u, about 80% of the total cross section comes from electron capture into the ground state. As expected, the cross sections for capture into the $n = 3, 4,$ and 5 shells of the He^+ ion are in decreasing order. The cross sections for capture into the $n = 5$ shell show the lowest contribution and are smaller than the results for the ground state by more than two orders of magnitude in the entire energy range considered. The present results are compared with the BCIS-3B ones by Delibašić *et al.* [37]. While there is good agreement between the two methods at high energies, there is significant deviation below 100 keV/u, which is especially noticeable for electron capture into the ground state.

B. Elastic scattering and excitation

The WP-CCC cross sections for elastic scattering and target excitation into the $2l$ and $3l$ states are shown in Fig. 7. For target excitation, the AOCC calculations of Fritsch [43] are also shown. The figure reveals that elastic scattering is

TABLE I. Cross sections for electron capture into the $n = 1-5$ shells in $\text{He}^{2+}\text{-He}(1s^2)$ collisions (in 10^{-16} cm^2). The WP-CCC results are compared with the BCIS-3B ones by Delibašić *et al.* [37]. The last column shows the corresponding total electron-capture cross section.

Energy (keV/u)	Method	$n = 1$	$n = 2$	$n = 3$	$n = 4$	$n = 5$	Total
15	WP-CCC	6.42×10^{-1}	1.33	7.81×10^{-2}	2.37×10^{-2}	9.97×10^{-3}	2.09
20	WP-CCC	7.99×10^{-1}	1.89	1.10×10^{-1}	3.00×10^{-2}	1.36×10^{-2}	2.89
	BCIS-3B	2.18×10^1	1.87×10^{-1}	2.26×10^{-2}	7.23×10^{-3}		2.20×10^1
30	WP-CCC	9.84×10^{-1}	2.23	2.68×10^{-1}	7.76×10^{-2}	3.83×10^{-2}	3.60
40	WP-CCC	1.04	1.94	3.68×10^{-1}	1.25×10^{-1}	6.52×10^{-2}	3.55
	BCIS-3B	8.47	7.47×10^{-1}	1.34×10^{-1}	4.63×10^{-2}		9.47
60	WP-CCC	9.46×10^{-1}	1.19	3.40×10^{-1}	1.37×10^{-1}	7.53×10^{-2}	2.69
	BCIS-3B	4.21	8.40×10^{-1}	2.03×10^{-1}	7.80×10^{-2}		5.46
80	WP-CCC	7.25×10^{-1}	7.16×10^{-1}	2.38×10^{-1}	1.03×10^{-1}	5.85×10^{-2}	1.84
	BCIS-3B	2.38	6.79×10^{-1}	1.94×10^{-1}	6.58×10^{-2}		3.45
100	WP-CCC	5.56×10^{-1}	4.43×10^{-1}	1.57×10^{-1}	7.05×10^{-2}	4.05×10^{-2}	1.26
	BCIS-3B	1.45	4.94×10^{-1}	1.55×10^{-1}	6.58×10^{-2}		2.27
150	WP-CCC	2.61×10^{-1}	1.55×10^{-1}	5.74×10^{-2}	2.64×10^{-2}	1.52×10^{-2}	5.15×10^{-1}
	BCIS-3B	5.28×10^{-1}	2.06×10^{-1}	7.13×10^{-2}	3.16×10^{-2}		8.86×10^{-1}
300	WP-CCC	3.98×10^{-2}	1.44×10^{-2}	5.17×10^{-3}	2.46×10^{-3}	1.38×10^{-3}	6.33×10^{-2}
	BCIS-3B	6.31×10^{-2}	2.19×10^{-2}	7.81×10^{-3}	3.51×10^{-3}		1.02×10^{-1}
500	WP-CCC	6.00×10^{-3}	1.65×10^{-3}	5.66×10^{-4}	2.70×10^{-4}	1.59×10^{-4}	8.65×10^{-3}
	BCIS-3B	9.42×10^{-3}	2.65×10^{-3}	9.13×10^{-4}	4.07×10^{-4}		1.40×10^{-2}
800	WP-CCC	1.01×10^{-3}	2.11×10^{-4}	7.10×10^{-5}	3.30×10^{-5}	1.78×10^{-5}	1.34×10^{-3}
	BCIS-3B	1.29×10^{-3}	2.95×10^{-4}	9.80×10^{-5}	4.30×10^{-5}		1.79×10^{-3}
1000	WP-CCC	4.19×10^{-4}	8.51×10^{-5}	2.78×10^{-5}	1.22×10^{-5}	6.43×10^{-6}	5.51×10^{-4}
	BCIS-3B	4.67×10^{-4}	9.77×10^{-5}	3.19×10^{-5}	1.39×10^{-5}		6.32×10^{-4}
2000	WP-CCC	1.57×10^{-5}	2.73×10^{-6}	8.68×10^{-7}	3.78×10^{-7}	1.97×10^{-7}	1.99×10^{-5}
	BCIS-3B	1.57×10^{-5}	2.63×10^{-6}	8.25×10^{-7}	3.55×10^{-7}		2.01×10^{-5}
3000	WP-CCC	1.99×10^{-6}	3.21×10^{-7}	1.01×10^{-7}	4.61×10^{-8}	2.47×10^{-8}	2.48×10^{-6}
	BCIS-3B	1.90×10^{-6}	2.91×10^{-7}	8.96×10^{-8}	3.83×10^{-8}		2.38×10^{-6}

the dominant direct-scattering channel in the entire energy region. Starting from 50 keV/u, the cross section for excitation into the $2p$ state becomes larger than all the other excitation cross sections, making this channel the most probable target-excitation channel at higher energies. Generally, it appears that within each shell, excitation into the p states becomes dominant at higher projectile energies.

We observe different levels of agreement between the two sets of calculations for different states. While below 40 keV/u the AOCC and WP-CCC partial excitation cross sections appear more or less to agree with the corresponding counterparts, at 65 keV/u they deviate substantially. For instance, the AOCC cross sections for $2s$ and $2p$ excitation are about 70% larger than the corresponding WP-CCC results. Disagreement is even bigger for $3p$ excitation. We note the present the cross sections for excitation into states with the largest orbital angular momentum show a minimum at small energies. For $2p$ and $3d$ states, the minima can also be seen in the AOCC calculations, though the density of the energy points used by Fritsch [43] is not sufficient to exhibit this feature clearly.

C. Single ionization

Finally, we consider ionization of the helium target. Figure 8 shows the present two-electron and EIE WP-CCC results for the integrated cross section for single ionization of helium in comparison with the corresponding experimental measurements [19,22,23,25,64], as well as the theoretical

calculations [35,38,39,42]. We note that both our methods include not only direct ionization of the target but also electron capture to the continuum of the projectile. The two-electron and EIE results agree well with each other at low- and high-energy regions. However, the EIE results somewhat overestimate the two-electron ones at the intermediate energies, the difference being especially noticeable around 150 keV/u, where the peak of the cross section is observed. Overall, the discrepancy between the two theories is within 15%.

Our results are generally similar in shape to the experimental data by Shah and Gilbody [22] and Shah *et al.* [23]. While they are in good agreement with the data at low and high energies, one can see a noticeable discrepancy at intermediate energies. Near the peak, the two-electron WP-CCC results overestimate the data from Shah *et al.* [23] by about 20%. This appears to be a systematic problem in practically all close-coupling approaches to ionization in ion-atom collisions (see Refs. [10,54,65–67]). The WP-CCC results are also in very good agreement with the experiment of Puckett *et al.* [25] in the energy range above 150 keV/u.

We note that our two-electron calculations agree very well with the experimental data of Knudsen *et al.* [19] available at three projectile energies (0.63, 1.44, and 2.31 MeV/u). At these energies, Barna *et al.* [38] provided the results of three distinct theoretical methods: the single-center close-coupling approach and two versions of the CTMC method, one based on the equivalent electron approximation and the other on the nonequivalent electron approximation. The CC results are

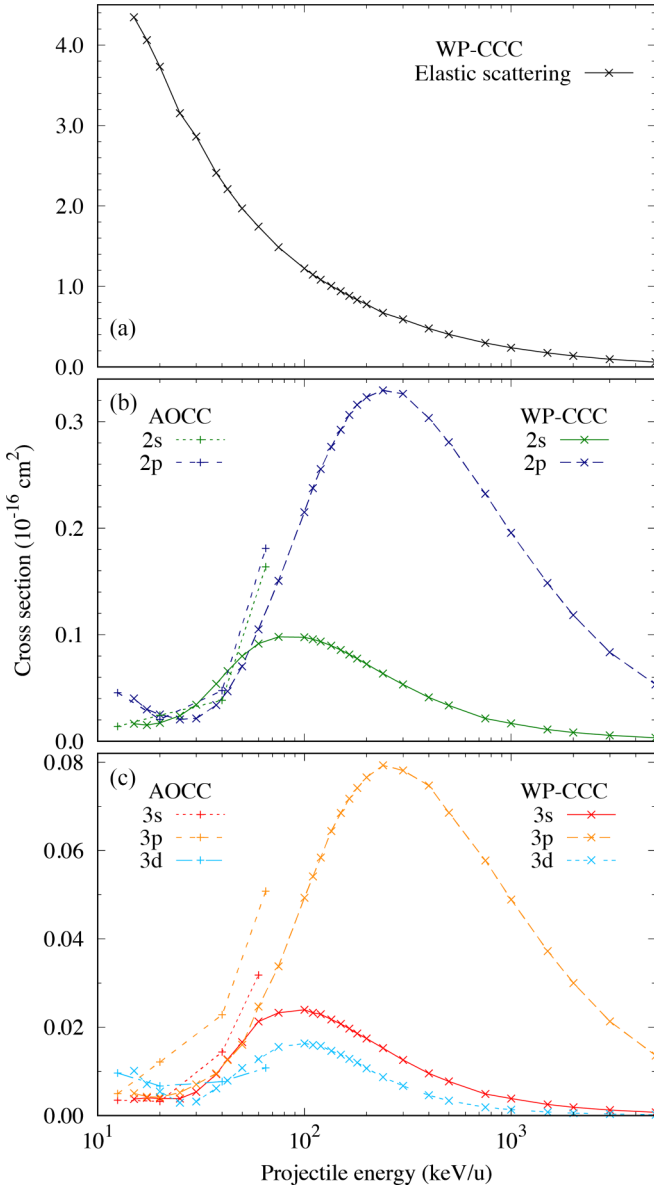


FIG. 7. Cross sections for (a) elastic scattering and target excitation into the (b) $2l$ and (c) $3l$ states in He^{2+} - $\text{He}(1s^2)$ collisions. The calculations of Fritsch [43] are also shown.

in excellent agreement with the experimental data and our calculations. However, both of the CTMC theories underestimate the experimental data, with the NEE-CTMC method agreeing better than the EE-CTMC one. Pindzola *et al.* [39] also performed single-center CC calculations at high energies. As expected, their results were practically identical to those by Barna *et al.* [38].

The TDDFT WB and TDDFT IEM methods by Baxter and Kirchner [42] were also applied to calculate the single-ionization cross section. We can see that the results obtained using the TDDFT WB approach agree with the TDDFT IEM calculations at low and high energies, but overestimate in the intermediate-energy region. The TDDFT WB calculations are in very good agreement with the available experimental data above 250 keV/u.

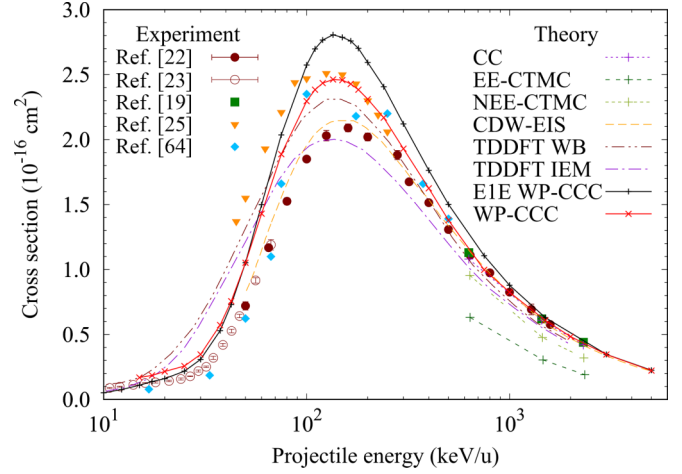


FIG. 8. Total cross section for single ionization in $\text{He}^{2+} + \text{He}(1s^2)$ collisions as a function of the incident projectile energy. The present WP-CCC and EIE WP-CCC results are represented by the red and black solid lines, respectively. The experimental data are due to Shah and Gilbody [22], Shah *et al.* [23], Puckett *et al.* [25], Knudsen *et al.* [19], and DuBois [64]. The other theoretical results are from the CC, EE-CTMC, and NEE-CTMC methods by Barna *et al.* [38], the CDW-EIS method by Terekhin *et al.* [35], and the TDDFT WB and TDDFT IEM methods by Baxter and Kirchner [42] with the MCHF wave function for He. The error bars reported in [22,23] are too small to be seen on this scale.

The 3B-CDW-EIS approach by Terekhin *et al.* [35] shows very good agreement with the data of Shah *et al.* In their approach, the four-body reaction is reduced to a three-body one, assuming the nonactive electron remains bound to the residual target throughout the collision. There are also calculations by Dunseath and Crothers [11] available for this collision system (they are not shown in the figure). They applied the continuum-distorted-wave approach using the Pluinage wave functions to derive the ionization amplitude for evaluating the cross section. Overall, these calculations do not agree with the experimental data either quantitatively or in shape. Also, the method failed to predict the maximum observed in the experiments [22,23,25] and in the other theoretical calculations that cover the energy region around 150 keV/u.

IV. SUMMARY AND CONCLUSIONS

To summarize, we studied the four-body scattering problem of He^{2+} collisions with the helium atom using the wave-packet convergent close-coupling approach and a recently developed effective one-electron method. In both approaches, the continuum for all involved atoms was discretized into a number of bins to obtain the corresponding positive-energy pseudostates. In the two-electron approach the electron-electron correlation and electron-exchange effects, which are particularly important at low collision energies, were fully taken into account. The frozen-core approximation was employed to treat the target atom, which assumes that one of the helium electrons remains in the ground state of the He^+ ion throughout the collision. The effective single-electron method makes the collisional system more convenient in

terms of numerical calculations. In presenting the final results, the cross sections were checked for convergence in terms of the included target and projectile states.

We presented cross sections for total and state-selective electron capture, excitation, and single ionization of the target. The results are provided for the incident energies from 10 keV/u to 5 MeV/u, where one-electron processes are expected to dominate. Attention is focused on the intermediate-energy region where we find substantial deviations between various theoretical methods. Overall, our two approaches show fairly good consistency with each other for all considered processes. The cross sections for total and state-selective electron capture as well as for single ionization show good agreement with the available experimental results and other theoretical calculations. For total electron capture, we observe generally good agreement between our results and the experimental data throughout the entire energy range considered. However, discrepancies between various theoretical results for the total and state-selective electron-capture cross sections below 100 keV/u require more investigation using independent methods. For single ionization, excellent agreement with experiment is obtained at high and low energies, whereas at intermediate energies the agreement with the data remains somewhat unsatisfactory.

In general, it is concluded that both approaches presented in this work are able to describe the overall picture of all

underlying processes in He²⁺-He collisions in terms of the integrated cross sections. For electron capture and ionization processes, the correlated two-electron calculations show much better agreement with the available experimental data than the effective single-electron ones. In particular, our results demonstrate that accurate description of state-selective electron capture at intermediate and low energies requires proper account of the electron-electron correlations in the target treatment and electron-exchange effects between the reaction products in the electron-transfer channels. Overall, the obtained results lay a reliable foundation for modeling two-electron processes like transfer excitation and transfer ionization, as well as differential scattering and ionization in this four-body system.

ACKNOWLEDGMENTS

We acknowledge the resources and services of the National Computational Infrastructure and the Pawsey Supercomputer Centre. S.U.A., I.B., and A.S.K. acknowledge support from the Australian Research Council. C.T.P. acknowledges support through an Australian Government Research Training Program Scholarship. This work was part of the Coordinated Research Project carried out under the sponsorship of the International Atomic Energy Agency.

-
- [1] Dž. Belkić, *J. Math. Chem.* **47**, 1366 (2010).
 - [2] Dž. Belkić, I. Bray, and A. Kadyrov, *State-of-the-Art Reviews on Energetic Ion-Atom and Ion-Molecule Collisions* (World Scientific, Singapore, 2019).
 - [3] Michael Schulz, *Ion-Atom Collisions: The Few-Body Problem in Dynamic Systems* (de Gruyter, Berlin, 2019).
 - [4] I. B. Abdurakhmanov, A. S. Kadyrov, D. V. Fursa, I. Bray, and A. T. Stelbovics, *Phys. Rev. A* **84**, 062708 (2011).
 - [5] I. Mančev, N. Milojević, and Dž. Belkić, *Phys. Rev. A* **86**, 022704 (2012).
 - [6] I. B. Abdurakhmanov, A. S. Kadyrov, S. U. Alladustov, I. Bray, and K. Bartschat, *Phys. Rev. A* **100**, 062708 (2019).
 - [7] D. Zajfman and D. Maor, *Phys. Rev. Lett.* **56**, 320 (1986).
 - [8] X. Guan and K. Bartschat, *Phys. Rev. Lett.* **103**, 213201 (2009).
 - [9] I. Mančev and N. Milojević, *Phys. Rev. A* **81**, 022710 (2010).
 - [10] T. G. Winter, *Phys. Rev. A* **44**, 4353 (1991).
 - [11] K. M. Dunseath and D. S. F. Crothers, *J. Phys. B* **24**, 5003 (1991).
 - [12] Dž. Belkić, *Phys. Rev. A* **47**, 189 (1993).
 - [13] Dž. Belkić, *J. Phys. B* **26**, 497 (1993).
 - [14] Dž. Belkić, *Phys. Rev. A* **37**, 55 (1988).
 - [15] D. R. Schultz and R. E. Olson, *Phys. Rev. A* **38**, 1866 (1988).
 - [16] M. M. Sant'Anna, A. C. F. Santos, L. F. S. Coelho, G. Jalbert, N. V. de Castro Faria, F. Zappa, P. Focke, and Dž. Belkić, *Phys. Rev. A* **80**, 042707 (2009).
 - [17] M. Alessi, S. Otranto, and P. Focke, *Phys. Rev. A* **83**, 014701 (2011).
 - [18] M. E. Rudd, R. D. DuBois, L. H. Toburen, C. A. Ratcliffe, and T. V. Goffe, *Phys. Rev. A* **28**, 3244 (1983).
 - [19] H. Knudsen, L. H. Andersen, P. Hvelplund, G. Astner, H. Cederquist, H. Danared, L. Liljeby, and K. G. Rensfelt, *J. Phys. B* **17**, 3545 (1984).
 - [20] M. E. Rudd, T. V. Goffe, and A. Itoh, *Phys. Rev. A* **32**, 2128 (1985).
 - [21] N. V. de Castro Faria, F. L. Freire, and A. G. de Pinho, *Phys. Rev. A* **37**, 280 (1988).
 - [22] M. B. Shah and H. B. Gilbody, *J. Phys. B* **18**, 899 (1985).
 - [23] M. B. Shah, P. McCallion, and H. B. Gilbody, *J. Phys. B* **22**, 3037 (1989).
 - [24] V. Mergel, R. Dörner, J. Ullrich, O. Jagutzki, S. Lencinas, S. Nüttgens, L. Spielberger, M. Unverzagt, C. L. Cocke, R. E. Olson, M. Schulz, U. Buck, E. Zanger, W. Theisinger, M. Isser, S. Geis, and H. Schmidt-Böcking, *Phys. Rev. Lett.* **74**, 2200 (1995).
 - [25] L. J. Puckett, G. O. Taylor, and D. W. Martin, *Phys. Rev.* **178**, 271 (1969).
 - [26] L. J. Puckett and D. W. Martin, *Phys. Rev. A* **1**, 1432 (1970).
 - [27] O. Voitke, P. A. Závodszky, S. M. Ferguson, J. H. Houck, and J. A. Tanis, *Phys. Rev. A* **57**, 2692 (1998).
 - [28] V. A. Sidorovich, V. S. Nikolaev, and J. H. McGuire, *Phys. Rev. A* **31**, 2193 (1985).
 - [29] R. Singal and C. D. Lin, *J. Phys. B* **24**, 251 (1991).
 - [30] P. N. Abufager, A. E. Martínez, R. D. Rivarola, and P. D. Fainstein, *J. Phys. B* **37**, 817 (2004).
 - [31] Dž. Belkić, R. Gayet, and A. Salin, *Phys. Rep.* **56**, 279 (1979).
 - [32] Dž. Belkić, R. Gayet, J. Hanssen, I. Mančev, and A. Nuñez, *Phys. Rev. A* **56**, 3675 (1997).

- [33] I. Mančev, *Phys. Rev. A* **60**, 351 (1999).
- [34] A. E. Martínez, G. R. Deco, R. D. Rivarola, and P. D. Fainstein, *Nucl. Instrum. Methods Phys. Res. Sect. B* **34**, 32 (1988).
- [35] P. Terekhin, P. Montenegro, M. Quinto, J. Monti, O. Fojón, and R. Rivarola, *Nucl. Instrum. Methods Phys. Res. Sect. B* **408**, 150 (2017).
- [36] S. Samaddar, S. Halder, A. Mondal, C. R. Mandal, M. Purkait, and T. K. Das, *J. Phys. B* **50**, 065202 (2017).
- [37] D. Delibašić, N. Milojević, I. Mančev, and Dž. Belkić, *At. Data Nucl. Data Tables* **148**101530 (2022).
- [38] I. F. Barna, K. Tokési, and J. Burgdörfer, *J. Phys. B* **38**, 1001 (2005).
- [39] M. S. Pindzola, F. Robicheaux, and J. Colgan, *J. Phys. B* **40**, 1695 (2007).
- [40] V. J. Montemayor and G. Schiwietz, *Phys. Rev. A* **40**, 6223 (1989).
- [41] L. Meng, R. E. Olson, R. Dorner, J. Ullrich, and H. Schmidt-Bocking, *J. Phys. B* **26**, 3387 (1993).
- [42] M. Baxter and T. Kirchner, *Phys. Rev. A* **93**, 012502 (2016).
- [43] W. Fritsch, *J. Phys. B* **27**, 3461 (1994).
- [44] P. G. Davies and D. R. Flower, *J. Phys. B* **31**, 3639 (1998).
- [45] J. W. Gao, Y. Wu, N. Sisourat, J. G. Wang, and A. Dubois, *Phys. Rev. A* **96**, 052703 (2017).
- [46] B. Zygelman, D. L. Cooper, M. J. Ford, A. Dalgarno, J. Gerratt, and M. Raimondi, *Phys. Rev. A* **46**, 3846 (1992).
- [47] D. Rabli, M. Gargaud, and R. McCarroll, *Phys. Rev. A* **64**, 022707 (2001).
- [48] C. H. Liu, J. G. Wang, and R. K. Janev, *J. Phys. B* **45**, 235203 (2012).
- [49] I. B. Abdurakhmanov, A. S. Kadyrov, and I. Bray, *Phys. Rev. A* **94**, 022703 (2016).
- [50] N. W. Antonio, C. T. Plowman, I. B. Abdurakhmanov, I. Bray, and A. S. Kadyrov, *J. Phys. B* **54**, 175201 (2021).
- [51] A. M. Kotian, C. T. Plowman, I. B. Abdurakhmanov, I. Bray, and A. S. Kadyrov, *J. Phys. B* **55**, 115201 (2022).
- [52] N. W. Antonio, C. T. Plowman, I. B. Abdurakhmanov, I. Bray, and A. S. Kadyrov, *Phys. Rev. A* **106**, 012822 (2022).
- [53] I. B. Abdurakhmanov, A. S. Kadyrov, I. Bray, and K. Bartschat, *Phys. Rev. A* **96**, 022702 (2017).
- [54] S. U. Alladustov, I. B. Abdurakhmanov, A. S. Kadyrov, I. Bray, and K. Bartschat, *Phys. Rev. A* **99**, 052706 (2019).
- [55] K. H. Spicer, C. T. Plowman, I. B. Abdurakhmanov, A. S. Kadyrov, I. Bray, and S. U. Alladustov, *Phys. Rev. A* **104**, 032818 (2021).
- [56] K. H. Spicer, C. T. Plowman, I. B. Abdurakhmanov, S. U. Alladustov, I. Bray, and A. S. Kadyrov, *Phys. Rev. A* **104**, 052815 (2021).
- [57] C. T. Plowman, I. B. Abdurakhmanov, I. Bray, and A. S. Kadyrov, *Eur. Phys. J. D* **76**, 31 (2022).
- [58] C. T. Plowman, I. B. Abdurakhmanov, I. Bray, and A. S. Kadyrov, *Eur. Phys. J. D* **76**, 129 (2022).
- [59] I. Mančev, N. Milojević, and Dž. Belkić, *At. Data Nucl. Data Tables* **102**, 6 (2015).
- [60] I. B. Abdurakhmanov, K. Massen-Hane, S. U. Alladustov, J. J. Bailey, A. S. Kadyrov, and I. Bray, *Phys. Rev. A* **98**, 062710 (2018).
- [61] J. Faulkner, I. B. Abdurakhmanov, S. U. Alladustov, A. S. Kadyrov, and I. Bray, *Plasma Phys. Contr. Fusion* **61**, 095005 (2019).
- [62] S. Alladustov, Ph.D. thesis, Curtin University, 2019.
- [63] I. B. Abdurakhmanov, C. T. Plowman, K. H. Spicer, I. Bray, and A. S. Kadyrov, *Phys. Rev. A* **104**, 042820 (2021).
- [64] R. D. DuBois, *Phys. Rev. A* **36**, 2585 (1987).
- [65] I. B. Abdurakhmanov, A. S. Kadyrov, S. K. Avazbaev, and I. Bray, *J. Phys.: Conf. Ser.* **635**, 022100 (2015).
- [66] H. A. Slim, E. L. Heck, B. H. Bransden, and D. R. Flower, *J. Phys. B* **24**, L421 (1991).
- [67] N. Toshima, *Phys. Rev. A* **59**, 1981 (1999).